VALIDATION OF SEISMIC DESIGN PROVISIONS FOR DIAPHRAGMS AND ASSESSMENT OF HIGHER-MODE RESPONSES ON EARTHQUAKE-RESISTANT BUILDINGS

C. Franco Mayorga and Georgios Tsampras

Department of Structural Engineering
University of California San Diego

Abstract

This research utilizes recorded strong-motion acceleration data to assess the Alternative Design Provisions for Diaphragms per ASCE/SEI 7-22 Section 12.10.3. The design acceleration coefficients computed using the Alternative Design Provisions are compared with the peak floor accelerations in buildings included in the California Strong Motion Instrumentation Program. Buildings within the California Geological Survey Network with recorded maximum peak floor accelerations larger than 0.2g are considered. Preliminary observations on the magnitude and distribution of the design acceleration coefficients over the height of buildings are presented.

Introduction

Floor diaphragms and their connections to the vertical elements of the seismic force-resisting systems are critical components of earthquake-resistant buildings. Underestimating the level of seismic-induced horizontal forces to which the diaphragms are subjected to could be catastrophic. The loss of the ability of the connections of diaphragms to transfer forces to the seismic force-resisting system could lead to local collapse of the floor or complete collapse of the building. More specifically, diaphragm collapses were observed after the Northridge earthquake due to the loss of connections between floor diaphragms and the vertical elements of precast concrete buildings and the vertical elements of tilt-up-wall buildings (Fleischman et al. (2013), Iverson and Hawkins (1994), Tilt-up-Wall Buildings (1996)). After the 2010-2011 Christchurch earthquakes, excessive damage and collapse of floor diaphragms were attributed to inadequate integrity of the load path, underestimation of seismic-induced horizontal forces, and poorly understood interactions between floor diaphragms and walls, supporting beams, and reinforced concrete (RC) moment frames (Gonzalez et al. (2017), Scarry (2014), Kam et al. (2011)). The complex interactions between diaphragms and other structural elements results to unpredictable seismic response of buildings which often lead to damage of structural members that are designed to remain undamaged (Kam et al. (2011), Bull (2004), Wallace et al. (2012), Henry et al. (2017)).

Earthquake numerical simulations of buildings have shown that the seismic-induced horizontal forces in floor diaphragms can be large relative to the strength of the floor diaphragms. These excessive forces can lead to an inelastic and potentially non-ductile response of the diaphragms (Fleischman and Farrow (2001)). The contribution of second and higher mode responses in the total dynamic response of buildings (termed higher mode effects) may contribute to the excessive forces and floor total accelerations (Sewell et al. (1986), Chopra

(2007)). For instance, it has been shown that high floor accelerations due to the higher mode effects can be expected in buildings with seismic force-resisting systems that develop a flexural yield mechanism at the base, such as flexural-dominant RC structural walls (Chopra (2007), Priestley and Amaris (2012), Wiebe sand Christopoulos (2009), Panagiotou and Restrepo (2009), Tsampras (2016)).

The Alternative Design Provisions for Diaphragms per ASCE/SEI 7-22 Section 12.10.3 provide estimates of the seismic-induced horizontal forces that can be used to design floor diaphragms. These force estimates were developed based on analysis of experimental data from shaking table tests (Panagiotou et al. (2011), Chen et al. (2016)) and earthquake numerical simulations (Choi et al. (2008), Fleischman (2013)). These force estimates consider the higher mode effects. Thus, it is expected that they should result in a more accurate estimate of the seismic-induced horizontal forces for the design of floor diaphragms.

Recently, the California Strong Motion Instrumentation Program (CSMIP) funded a project that aims to utilize recorded acceleration data to validate the seismic design provisions for diaphragms and assess the effect of higher-mode responses on the seismic response of earthquake-resistant buildings. This paper presents preliminary analysis results of the ongoing project. The design equations per ASCE/SEI 7-22 Section 12.10.3 are summarized. A preliminary assessment of the effect of the design parameters N, R, Ω_0, and z_s (defined later) on the design acceleration coefficients for an assumed structural system is presented. The instrumented buildings under consideration in this preliminary analysis are introduced. Buildings within the California Geological Survey Network (CE) that have more than 12 stories and have been subjected to maximum peak floor accelerations larger than 0.2g are considered in this preliminary analysis. A method that is available in the literature (Şafak and Çelebi 1990) is used to estimate the location of the center of rigidity over the height of a building. This method is validated by replicating calculations given in Şafak and Çelebi (1990). The recorded acceleration data used in this preliminary analysis are transformed to the center of rigidity. A comparison between the design acceleration coefficients and transformed measured peak floor accelerations is performed. Conclusions based on the preliminary analysis results are presented.

ASCE/SEI 7-22 Section 12.10.3 Alternative Design Provisions for Diaphragms

In-plane seismic design forces for diaphragms, including chords, collectors, and their connections to the vertical elements are given in Section 12.10.3 Alternative Design Provisions for Diaphragms of the ASCE/SEI 7-22. The in-plane seismic design forces are defined as

$$F_{px} = \frac{C_{px}}{R_s} w_{px} \geq 0.2\ S_{DS} I_e w_{px} \tag{1}$$

where C_{px} is the design acceleration coefficient at level x, w_{px} is the weight tributary to the diaphragm at level x, R_s is the diaphragm design force reduction factor, S_{DS} is the design, 5% damped, spectral response acceleration parameter at short periods, and I_e is the building importance factor. The distribution of design acceleration coefficients over the normalized building height is presented in Figure 1. In this figure, N is the number of stories above the base, h_x is the height above the base to the level x, h_n is the vertical distance from the base to the highest level of the seismic force-resisting system (SFRS) of the structure, and C_{p0} is the diaphragm acceleration coefficient at the base. C_{p0} is computed as

$$C_{p0} = 0.4 S_{DS} I_e \tag{2}$$

C_{pi} is the diaphragm design acceleration coefficient at 80% of h_n calculated as

$$C_{pi} = \max\left(0.8 C_{p0}, 0.9 \Gamma_{m1} \Omega_0 C_s\right) \tag{3}$$

where $\Gamma_{m1} = 1 + z_s(1 - 1/N)/2$ is the first modal contribution factor, Ω_0 is the overstrength factor, and C_s is the seismic response coefficient in accordance with Section 12.8.1.1 of the ASCE/SEI 7-22. The term C_{pn} is the diaphragm design acceleration coefficient at h_n computed as

$$C_{pn} = \sqrt{(\Gamma_{m1} \Omega_0 C_s)^2 + (\Gamma_{m2} C_{s2})^2} \geq C_{pi} \tag{4}$$

where

$$C_{s2} = \begin{cases} \min\left(\frac{I_e S_{D1}}{0.03(N-1)}; (0.15N + 0.25) I_e S_{DS}; I_e S_{DS}\right), & N \geq 2 \\ 0, & N = 1 \end{cases} \tag{5}$$

is the higher mode seismic response coefficient and $\Gamma_{m2} = 0.9 z_s (1 - 1/N)^2$. N was previously defined and z_s is the mode shape factor defined in Section 12.10.3.2.1 of the ASCE/SEI 7-22.

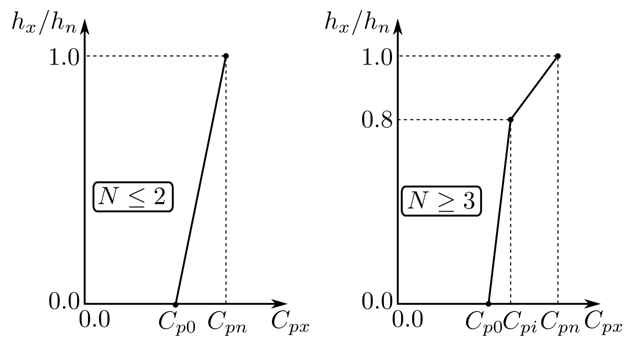

Figure 1 Calculation of the design acceleration coefficients in buildings with N ≤ 2 and in buildings with N ≥ 3 (Figure 12.10-2 in ASCE/SEI 7-22)

Effect of Parameters N, R, Ω_0, and zs

This section presents the effect of the primary design parameters in the values of C_{px}. An example building with constant story height of 10.0 [ft] is assumed. $S_s = 1.93[g]$ and $S_1 = 0.75[g]$, and Class D site as defined in ASCE/SEI 7-22 are also assumed. The varying parameters are the following: $N = 10, 20, 30, 40, 50$, $R = 4.0, 4.5, 5.0, 5.5., 6.0$, $\Omega_0 = 2.0, 2.2, 2.4, 2.6, 2.8, 3.0$ and $z_s = 0.3, 0.7, 0.85, 1.0$. The results of the sensitivity analysis are shown in Figure 2 for $R_s = 1$. The first plot shows the results for varying N and constant $R = 5.0$, $\Omega_0 = 2.6$, and z_s=1.0. The second plot shows the results for varying R and constant $N = 20$,

$\Omega_0 = 2.6$, and z_s=1.0. The third plot shows the results for varying Ω_0 and constant $N = 20$, $R = 5.0$, and z_s=1.0. The fourth plot shows the results for varying z_s and constant $N = 20$, $R = 5.0$, and $\Omega_0 = 2.6$.

The fundamental period of the structure is estimated using the equations given in Section 12.8.2.1 of the ASCE/SEI 7-22. This fundamental period is used to compute the seismic response coefficient C_s from the design acceleration spectrum. As N increases the fundamental period increases, C_s at the fundamental period decreases and, as a result, C_{px} overall decreases as shown in Figure 2. As N increases Γ_{m1} and Γ_{m2} tend to $1 + z_s/2$ and $0.9z_s$, respectively, as shown in Figure C12.10-3 in ACSE 7-16 Section C12.10.3.2. Note that there is a considerable reduction of the parameter C_{pi} from $N = 20$ to $N = 30$. For $N \geq 30$, the variation of C_{pi} with respect to N is not appreciable. The variation of C_s with respect to the value of period is lower within the range of longer periods, and consequently the variation of C_{pi} is lower within the range of longer periods. In addition, N also affects the higher mode seismic response coefficient C_{s2} governed by the term $I_e S_{D1}/0.03(N-1)$.

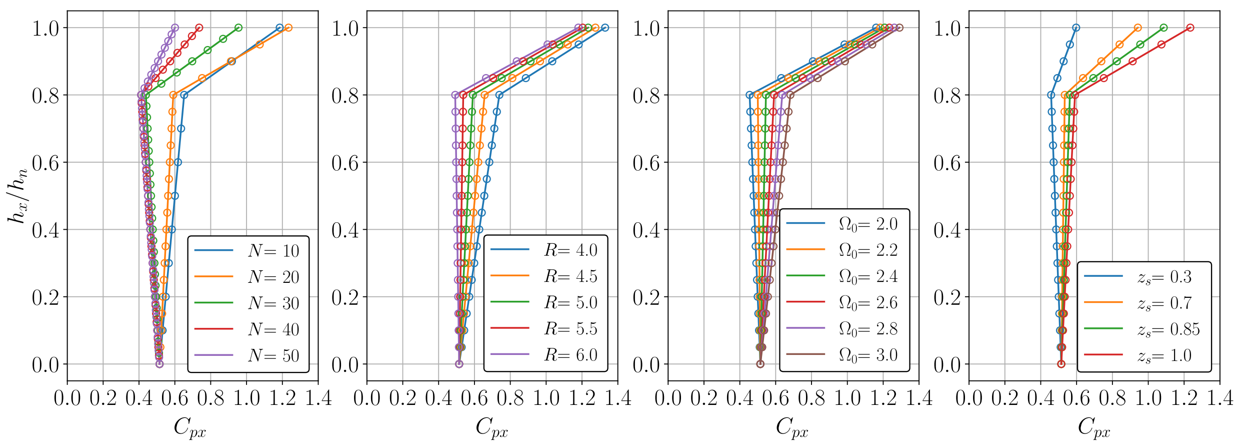

Figure 2 Design acceleration coefficients C_{px}. The number of stories N, the response modification factor of the structure R, the overstrength factor Ω_0, and the mode shape factor z_s effect

Parameters R and Ω_0 directly affect the contribution of the first mode to the C_{px} values. Figure 2 shows that an increase of R results to a reduction of the C_{px} values. An increase of Ω_0 results to an increase of the C_{px} values. These results are consistent with the fact that the inelastic response of SFRS (i.e., R is larger than 1) reduces the level of force responses in the building, and the overstrength in the inelastic response of SFRS increases the level of force responses in the building.

The mode shape factor z_s is positive linearly related to the modal contribution factors Γ_{m1} and Γ_{m2}. z_s affects more the value of Γ_{m2} compared to the value of Γ_{m1}. Therefore, an increase of z_s results to a higher increase in the value of C_{pn} compared to the value of C_{pi} as shown in Figure 2. z_s captures the differences in the distribution of inelastic deformation over the height of different types of seismic force-resisting systems (Section C12.10.3.2 of the ASCE/SEI 7-22).

Buildings Considered in Preliminary Analysis

A set of fourteen instrumented buildings that are part of the California Strong Motion Instrumentation Program (CSMIP) were selected to compare their peak floor accelerations to the design acceleration coefficients defined in the previous section. More specifically, the buildings considered in this preliminary study have more than 12 stories, they were designed assuming risk category II, and soil class D and C, they belong in the California Geological Survey Network (CE), and they have been subjected to ground motions that resulted to recorded floor accelerations larger than 0.2g. Twenty cases of analysis that consider unique combinations of building stations and seismic events are defined in Table 1. Table 1 lists the station of measurement, recorded seismic event, design date, design code, number of stories, building risk category, site class, spectral response acceleration parameter at short periods S_s, and spectral response acceleration parameter at a period of 1 [s] S_1 for each analysis case. These spectral acceleration parameters are obtained based on the building location in terms of latitude and longitude given on the Center for Engineering Strong Motion Data (CESMD) website https://www.strongmotioncenter.org/ and the risk category defined in terms of the building use or occupancy.

Table 1 Analysis case, station of measurement, recorded seismic event, design date, design code, number of stories, building risk category, site class, spectral response acceleration parameter at short periods S_s, and spectral response acceleration parameter at a period of 1 [s] S_1

Case	Station	Recorded seismic event	Design date	Design code**	No. of stories*	Risk Category	Soil Class	S_s[g] *****	S_1[g] *****
1	CE14654	Northridge (1994)	1985	UBC-82	14	II	D	1.851	0.652
2	CE24236	Whittier (1987)	1925	--	14	II	D	2.092	0.750
3	CE24322 ***	Northridge (1994)	1964	--	13	II	D	1.962	0.700
4	CE24322	Encino (2014)	1964	--	13	II	D	1.962	0.700
5	CE24464	Northridge (1994)	1967	LABC-66	20	II	C	2.082	0.747
6	CE24566	Northridge (1994)	1971	--	12	II	C	2.090	0.762
7	CE24569	Northridge (1994)	1961	LABC-60	15	II	C	1.993	0.710
8	CE24601	Landers (1992)	1980	--	17	II	C	1.978	0.705
9	CE24601	Northridge (1994)	1980	--	17	II	C	1.978	0.705
10	CE24602	Sierra Madre (1991)	1988-90	--	52	II	C	1.967	0.700
11	CE24602	Northridge (1994)	1988-90	--	52	II	C	1.967	0.700
12	CE24602	Chino Hills (2008)	1988-90	--	52	II	C	1.967	0.700
13	CE24643	Northridge (1994)	1967	--	19	II	D	2.082	0.744
14	CE24643	Northridge (1994)	1967	--	19	II	D	2.082	0.744
15	CE24680	Encino (2014)	1965	LABC-64	14	II	D	2.270	0.720
16	CE57357	Mt. Lewis (1986)	1972	--	13	II	D	1.530	0.523
17	CE57357 ****	Loma Prieta (1989)	1972	--	13	II	D	1.530	0.523
18	CE58480	Loma Prieta (1989)	1964	--	18	II	D	1.500	0.600
19	CE58483	Loma Prieta (1989)	1964	--	24	II	C	1.802	0.686
20	CE58639	Berkeley (2018)	1975	UBC-73	13	II	C	1.865	1.865

* Number of stories above the ground level
** Design code given in the building station websites. UBC: Uniform Building Code. LABC: Los Angeles Building Code.
*** The building was strengthened with friction dampers after the 1994 Northridge Earthquake.
**** 96 dampers were installed after the Loma Prieta Earthquake to reduce building movement.
***** S_s and S_1 are obtained based on the building location and Risk Category.

Based on the design date (and design code when available), seismic force-resisting systems (SFRS) defined in Table 12.2-1 of the ASCE/SEI 7-22 are assumed for the analysis cases given in Table 1. Table 2 lists the assumed seismic force-resisting system, the corresponding response modification coefficient R, and overstrength factor Ω_0. The considered SFRS are: Precast RC shear walls (SFRS A5), steel concentrically braced frames (SFRS B2), steel moment-resisting frames (SFRS C3), RC moment-resisting frames (SFRS C6), and dual systems (steel concentrically braced frames and moment-resisting frames (SFRS E1), and RC shear walls and moment-resisting frames (SFRS E8)). Additionally, Table 2 lists the approximate fundamental period used to compute the seismic response coefficient C_s. These periods are estimates of the actual periods of the buildings based on approximate equation provided in ASCE/SEI 7-22. In future work, the authors are planning to estimate the periods using identification methods based on the recorded data (Moaveni et al. (2011), Harris et al. (2015), Xiang et al. (2016), Astroza et al. (2016)).

Table 2 Assumed seismic force-resisting systems, response modification coefficients R, overstrength factors Ω_0, and the approximated fundamental periods T

Case	Assumed Seismic Force-Resisting System (SFRS)*	Response modification factor R	Overstrength factor Ω_0	Approximated fundamental period $T \approx c_u T_a$ [s]
1	E1	6.0	2.5	1.421
2	E8	5.5	2.5	1.193
3	C6	5.0	3.0	2.206
4	C6	5.0	3.0	2.206
5	C6	5.0	3.0	2.572
6	C3	4.5	3.0	2.363
7	C3	4.5	3.0	2.825
8	A5	4.0	2.5	1.198
9	A5	4.0	2.5	1.198
10	B2	6.0	2.0	3.876
11	B2	6.0	2.0	3.876
12	B2	6.0	2.0	3.876
13	C3	4.5	3.0	3.454
14	B2	6.0	2.0	1.865
15	E8	5.5	2.5	1.266
16	C3	4.5	3.0	2.564
17	C3	4.5	3.0	2.564
18	C3	4.5	3.0	3.036
19	E8	5.5	2.5	1.594
20	A5	4.0	2.5	0.976

* The SFRS nomenclature refers to Table 12.2-1 of the ASCE/SEI 7-22.
** The upper limit of the approximated fundamental period $c_u T_a$ given in Section 12.8.2.1 of the ASCE/SEI 7-22 is used as the fundamental period T in the computation of the seismic response coefficient C_s.

It is noted that at this time the preliminary analysis considers a limited number of buildings. The authors will expand the scope of the analysis to include a larger number of buildings.

Estimation of Floor Accelerations at the Center of Rigidity

The torsional component of the seismic response of buildings may contribute to the floor total accelerations measured away from the center of rigidity of the buildings (e.g., sensor 18 on the 49th floor of the CE24602 building station shown in Figure 3). This contribution of the torsional response to the floor total acceleration is more important for buildings with asymmetric floor plans in which the center of mass is expected to be located eccentrically with respect to the center of rigidity. In this study, the recorded floor total accelerations are decomposed to two horizontal translational components of accelerations and one torsional component of accelerations at the center of rigidity. At the center of rigidity, the horizontal translational floor accelerations are theoretically independent of the torsional floor accelerations. In this study, C_{px} values are compared to the horizontal translational accelerations computed at the center of rigidity using the accelerations measured at the location of the sensors.

The location of the center of rigidity at a floor of a building primarily depends on the elastic properties of the structural system. However, the actual location of the center of rigidity is affected by the nonstructural components and the inelastic response of the building. Şafak and Çelebi (1990) proposed a method to compute the center of rigidity from recorded acceleration data. This method is used to compute the location of the center of rigidity in this paper.

Theoretically, the translational motions are not correlated with the torsional motion at the center of rigidity. However, due to measurement errors and considering the possibility of having coupled translational-torsional modes in buildings, the cross-correlation is different to zero when recorded translational floor accelerations and torsional floor accelerations are compared. Based on this, Şafak and Çelebi relaxed the condition of zero cross-correlation. Şafak and Çelebi proposed to minimize the cross-correlation in function of the feasible coordinates of the center of rigidity.

To apply the method proposed by Şafak and Çelebi (1990), the measurements must satisfy the following conditions: (1) At least three measurements are required; (2) the measurements should be obtained from a minimum of two different point locations on the floor; (3) the directions of the measurements should not intersect at one point; and (4) the directions of measurements should not be parallel. Then, it is assumed that the data is measured at points P and Q with coordinates (x_p, y_p) and (x_q, y_q), respectively. Considering that the seismic response of the building results in torsion that can be assumed to be small (i.e., small angle approximation), the translational and torsional motions of a point G (x_g, y_g) located in another point on the floor plane can be computed as

$$\begin{aligned} U_g &= U_p + (y_p - y_g)\theta \\ V_g &= V_p - (x_p - x_g)\theta \end{aligned} \tag{6}$$

where (U_p, V_p) and (U_g, V_g) are the translational motions of the points P and G, respectively, and $\theta = -(U_p - U_q)/(y_p - y_q) = (V_p - V_q)/(x_p - x_q)$ is the floor torsional rotation (independent of the coordinate reference). Note that, for the implemented criterion, G is considered equal to the center of rigidity when the cross-correlation between U_g and θ termed $R_{U_g\theta}(t,\tau)$, or the cross correlation between V_g and θ termed $R_{V_g\theta}(t,\tau)$, are minimum. In general, the cross-correlation for nonstationary functions is a function of both time t and correlation lag τ , however, it is assumed that $R_{U_g\theta}$ and $R_{V_g\theta}$ are functions of τ only. Alternatively in the frequency domain, the coherence function between U_g and θ termed $\Gamma_{U_g\theta}(f)$, or the coherence function between V_g and θ termed $\Gamma_{V_g\theta}(f)$, can be minimized to find the location of the center of rigidity. At the center of rigidity these motions are expected to be incoherent, but the results could be affected by the frequency content. Şafak and Çelebi (1990) proposed to use the area under the coherence function as an approximate frequency-independent measure defined as shown below

$$L_{U_g\theta} = \int_0^\infty \Gamma^2_{U_g\theta}(f)\,df \quad \text{and} \quad L_{V_g\theta} = \int_0^\infty \Gamma^2_{V_g\theta}(f)\,df \tag{7}$$

where

$$\Gamma^2_{U_g\theta}(f) = \frac{\left|S_{U_g\theta}(f)\right|^2}{S_{U_gU_g}(f)S_{\theta\theta}(f)} \quad \text{and} \quad \Gamma^2_{V_g\theta}(f) = \frac{\left|S_{V_g\theta}(f)\right|^2}{S_{V_gV_g}(f)S_{\theta\theta}(f)} \tag{8}$$

and $S_{lm}(f)$ is the cross-spectrum of the corresponding l and m signals (power spectra or auto-spectra when $l = m$).

Figure 4 shows the results of the calculation of the coherence area that are used to estimate the center of rigidity of the 49th floor of the building station CE24602 (see Figure 3) for the recorded seismic events: Sierra Madre (1991), Northridge (1994), and Chino Hills (2008) (cases 10, 11, 12, respectively, in Table 1). The sensor coordinates with respect to the center of geometry of the floor plan are estimated from the schematics shown in Figure 3. Table 3 lists the coordinates that minimize the coherence areas for each seismic event. These coordinates are estimates of the coordinates of the center of rigidity for each seismic event. As expected, the actual location of the center of rigidity depends on the considered seismic event. The estimate of y_g coordinate is similar using accelerations from the three seismic events (between 4.68 [ft] and 6.24 [ft]). The estimate of x_g coordinate is 24.96 [ft] considering the seismic event Sierra Madre (1991) and it shifts to 35.88[ft] considering the seismic event Northridge (1994).

Table 3 Coordinates of the center of rigidity of the 49th story

Case	Seismic event	Center of rigidity coordinates	
		x_g [ft]	y_g [ft]
10	Sierra Madre (1991)	24.96	4.68
11	Northridge (1994)	35.88	6.24
12	Chino Hill (2008)	35.88	4.68

In the case in which an instrumented floor has only two orthogonal measurements, such as the 14th floor of the CE24602 building station shown in Figure 3, the torsional rotation cannot be computed. In these cases, the two orthogonal measurements of acceleration are used in this preliminary study.

In the future, the authors are planning to compare the results obtained from the presented method used to estimate the location of the center of rigidity against the location of the center of rigidity estimated using the structural floor plans of buildings.

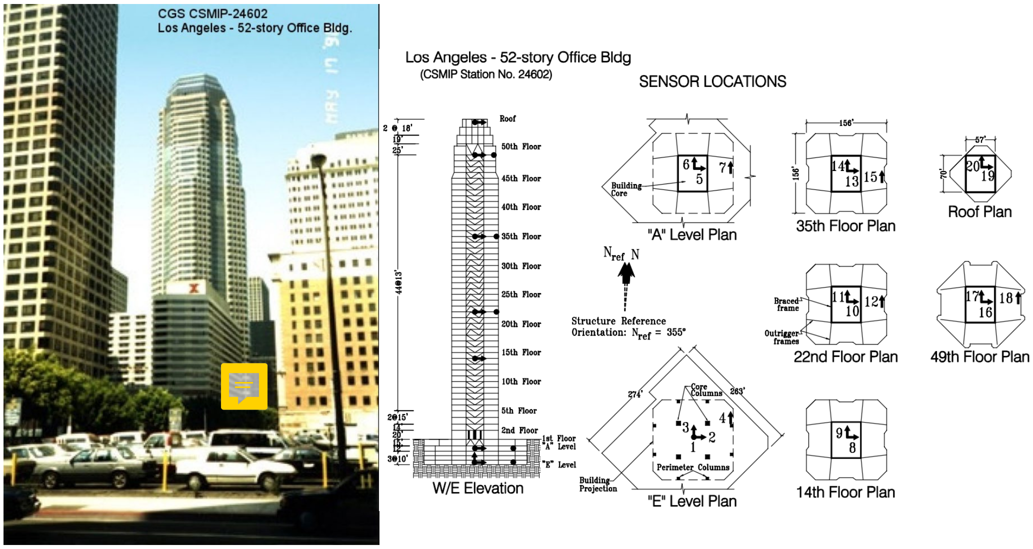

Figure 3 Cases 10, 11, and 12: moment frame building (https://www.strongmotioncenter.org/cgi-bin/CESMD/stationhtml.pl?stationID=CE24602&network=CGS)

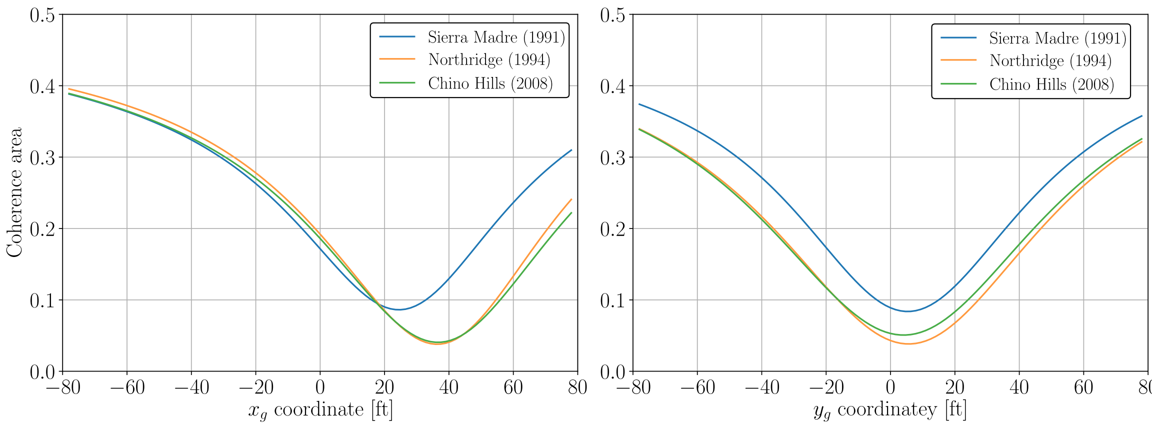

Figure 4 Coherence area versus trial center of rigidity coordinates of the 49th floor. Caso 10: Sierra Madre earthquake (1991), Case 11: Northridge earthquake (1994), and Case 12: Chino Hill earthquake (2008)

Comparison between Design Acceleration Coefficients and Measured Peak Floor Accelerations

Once the responses at the center of rigidity are obtained, the peak horizontal floor accelerations at the instrumented floors are computed. The objective of this preliminary analysis is to compare the magnitude of the peak floor accelerations with the C_{px} values and graphically identify the floors in which higher amplifications of recorded peak floor accelerations with respect to the peak ground accelerations are observed. The preliminary analysis does not compare the distribution of peak floor accelerations over the height of the building with the distribution of C_{px} values over the height of the building. This is because the inelastic response of buildings expected under the design level ground motions may limit the higher mode effects on the peak floor accelerations. Therefore, a comparison between the distribution of peak floor accelerations and the distribution of C_{px} values over the height of the building requires recorded ground motions with intensities close to the seismic design level intensity. Most of the buildings considered in this preliminary analysis are not subjected to recorded ground motions with intensities close to the design level intensity. Nevertheless, additional buildings in the CSMIP dataset with recorded total accelerations close to the design level intensity will be included in future analysis. For these additional buildings, the distribution of peak floor accelerations versus the distribution of C_{px} values will be compared.

Figure 5 shows the distribution of the peak floor accelerations and the corresponding values of C_{px} over the normalized height of the buildings. Figure 5 shows the results for each analysis case grouped based on the seismic force-resisting system of each building. The square and triangular markers represent the peak floor accelerations in x and y directions, respectively. The solid circular markers are the corresponding C_{px} values for the analysis cases. Analysis cases 3 and 4; 8 and 9; 10, 11, and 12; and 16 and 17 correspond to the same building station subjected to different seismic event. Thus, the C_{px} values for these analysis cases overlap. Cases 13 and 14 correspond to the same building station but with different seismic force-resisting system per direction of analysis. In the longitudinal direction of this building the SFRS is a steel moment frame (SFRS C3) and in the transverse direction of this building the SFRS is a steel concentrically braced frame (SFRS B2). As a result, there are two different distributions of C_{px} values for this building. Table 4 lists the maximum ratio of the measured peak floor accelerations over the C_{px} values for all the analysis cases. This ratio is termed Maximum M/D ratio.

Table 4 Maximum floor acceleration Measured-Design (M/D) ratios

Case	Maximum M/D ratio	Case	Maximum M/D ratio
1	0.52	11	0.80
2	0.23	12	0.52
3	**1.56**	13	**1.25**
4	0.81	14	**1.24**
5	0.66	15	0.51
6	0.51	16	0.73
7	0.47	17	0.82
8	0.29	18	0.78
9	0.52	19	0.53
10	0.45	20	0.33

Figure 5 shows that the peak floor accelerations do not exceed the C_{px} values for most of the cases considered in this analysis, except for Cases 3, 4, and 13 which are discussed at the end of this section. Accordingly, all the M/D ratios presented in Table 4 are lower than one (except for Cases 3, 4, and 13). These results are consistent with the fact that the intensity of the recorded ground motions to which the buildings were subjected to are lower than the seismic design level intensity. Thus, if these buildings had been designed following the current alternative design provisions for diaphragms, the induced inertial forces for the recorded seismic events would have been expected to be lower than the diaphragm design strengths.

Figure 5 shows an amplification in the peak total accelerations at the higher floors of the buildings that are subjected to the larger ground motion intensities in the SFRS A5 and B2 analysis cases. Similar amplification is observed in the peak total accelerations along the x-

direction in Cases 5 and 19 that correspond to SFRS C6 and E8, respectively. This amplification is not identified in the SFRS C3 analysis cases.

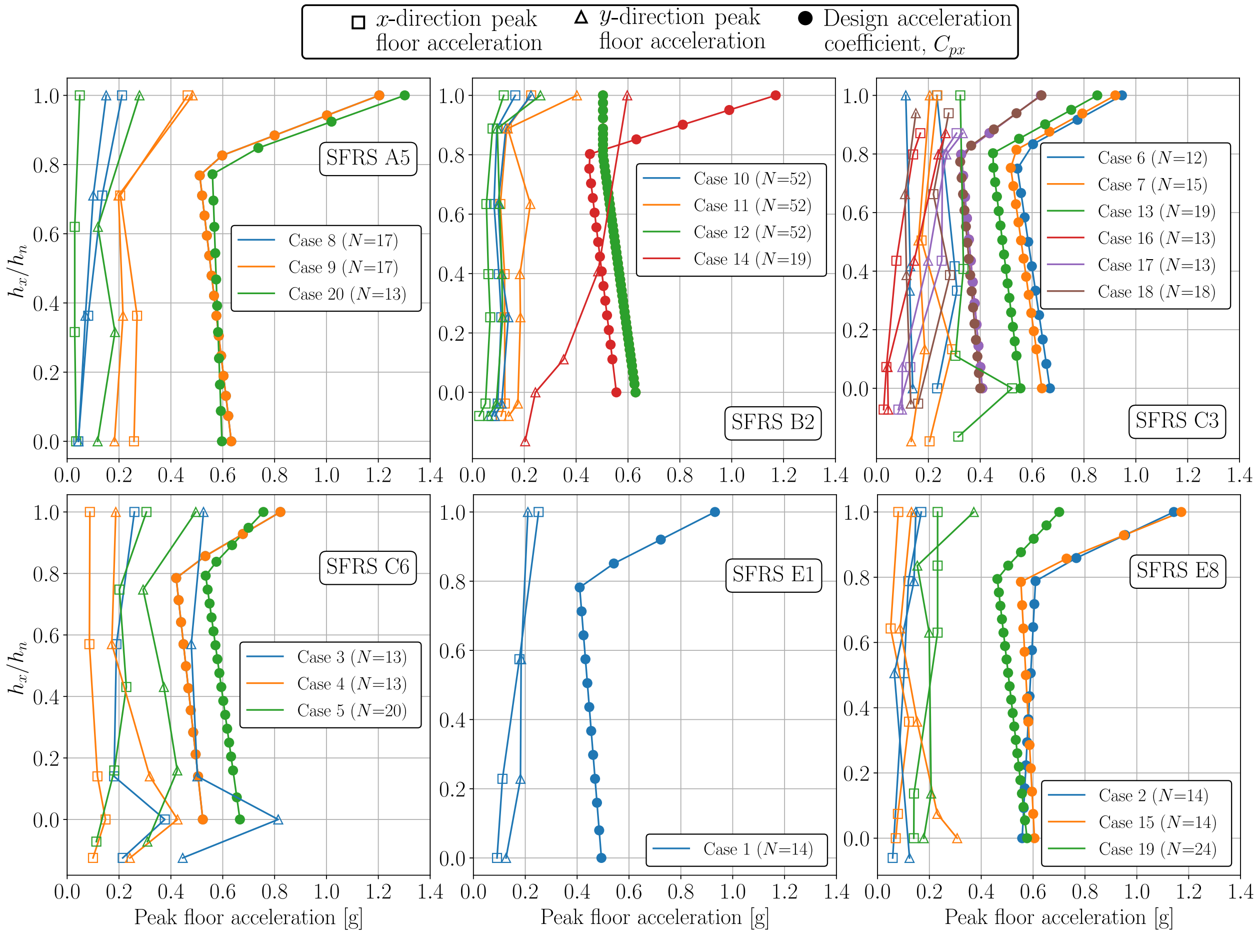

Figure 5 Diaphragm design acceleration coefficients versus peak floor accelerations at the center of rigidity comparison.

Cases 10, 11 and 12 correspond to the same building station (CE24602) subjected to three different recorded ground motions (Sierra Madre (1991), Northridge (1994), and Chino Hills (2008)). These analysis cases demonstrate that the distribution of peak floor accelerations over the height of the building depends on the intensity of the ground motions. A larger amplification in the roof acceleration is observed in the upper floors in the y-direction of Case 11 compared to the other two analysis cases. Case 11 corresponds to the recorded seismic event with the largest seismic intensity for this building station (Northridge seismic event). The authors are currently working on the comparison of the seismic-induced spectral accelerations with the design spectral accelerations.

The maximum peak floor accelerations were recorded at the second floor in Cases 3, 4, and 13. The distribution of peak floor accelerations over the height of the building in Case 14 abruptly increased after the first floor. The observations associated with the above-mentioned analysis cases are attributed to the structural irregularities over the height of the buildings. Performance-based assessment of these buildings could be used to estimate the diaphragm design forces.

Conclusions

This paper presented a summary of the ASCE 7-22 alternative design provisions for diaphragms. Results from a limited sensitivity analysis of the design acceleration coefficients (C_{px}) with respect to parameters N, R, Ω_o, and z_s were presented. The instrumented buildings considered in this preliminary analysis were introduced. A method to estimate the location of the center of rigidity over the height of a building using recorded acceleration data proposed by Şafak and Çelebi (1990) was introduced. A comparison between the values of the design acceleration coefficients and the measured peak floor accelerations transformed at the center of rigidity was performed.

The preliminary analysis shows that the recorded peak floor accelerations of the buildings in this study are generally smaller than the C_{px} values. The recorded peak floor accelerations in buildings with vertical irregularities were larger than the C_{px} values. The distribution of the peak floor accelerations over the height depends on the ground motion intensity. Future analyses will include larger number of buildings to derive detailed conclusions with respect to the recorded peak floor accelerations compared to the C_{px} values.

Acknowledgments

The authors acknowledge to the California Strong Motion Instrumentation Program for their support through the project called “Validation of Seismic Design Provisions for Diaphragms and Assessment of Higher-Mode Responses on Earthquake-Resistant Buildings” and to the Chilean National Agency for Research and Development (ANID) for their support through the foreign doctoral scholarship 2020. The authors also acknowledge to Mehmet Çelebi, PhD, PE and Lisa S. Schleicher, Ph.D., Geophysicist, both part of the USGS, for facilitating the data required to replicate the results given in Şafak and Çelebi (1990). Any opinions, findings, and conclusions expressed in this paper are those of the authors and do not necessarily reflect the views of others acknowledged here.

References

ASCE/SEI 7-22 (2021). Minimum design loads and associated criteria for buildings and other structures. *American Society of Civil Engineers*.

Astroza, Rodrigo, Ebrahimian, H., Conte, J. P., Restrepo, J. I., and Hutchinson, C. T. (2016). System Identification of a Full-Scale Five-Story Reinforced Concrete Building Tested on the NEES-UCSD Shake Table. *Structural Control and Health Monitoring* 23, no. 3: 535–59. https://doi.org/10.1002/stc.1778.

Bull, D. K. (2004). Understanding the Complexities of Designing Diaphragms in Buildings for Earthquakes. *Bulletin of the New Zealand Society for Earthquake Engineering* 37, no. 2: 70–88. https://doi.org/10.5459/bnzsee.37.2.70-88.

Chen, Michelle C., Pantoli, E., Wang, X., Astroza, R., Ebrahimian, H., Hutchinson, T.C., Conte, J.P., Restrepo, J. I., Marin, C., Walsh, K. D., Bachman, R.E., Hoehler, M.S., Englekirk, R., and Faghihi, M. (2016). "Full-Scale Structural and Nonstructural Building System Performance during Earthquakes: Part I – Specimen Description, Test Protocol, and Structural Response." *Earthquake Spectra* 32, no. 2: 737–70. https://doi.org/10.1193/012414eqs016m.

Choi, H., Christopoulos, C., and Tremblay, R. (2008). Comparison of the Seismic Response of Steel Buildings Incorporating Self-Centering Energy Dissipative Braces, Buckling Restrained Braced and Moment Resisting Frames. Research Report 05-2008, University of Toronto,Canada.

Chopra, Anil K (2007). *Dynamics of Structures*. Pearson Education.

Fleischman, R. B., and Farrow, K. T. (2001). Dynamic Behavior of Perimeter Lateral-System Structures with Flexible Diaphragms. *Earthquake Engineering & Structural Dynamics* 30, no. 5: 745–63. https://doi.org/10.1002/eqe.36.

Fleischman, R. B., Restrepo, J. I., Naito, C. J., Sause, R., Zhang, D., and Schoettler, M. (2013). "Integrated Analytical and Experimental Research to Develop a New Seismic Design Methodology for Precast Concrete Diaphragms." *Journal of Structural Engineering* 139, no. 7: 1192–1204. https://doi.org/10.1061/(ASCE)ST.1943-541X.0000734.

González, Alfredo, Spacone, E., and Nascimbene, R. (2017). Performance-Based Seismic Design Framework for RC Floor Diaphragms in Dual Systems. *Procedia Engineering*, X International Conference on Structural Dynamics, EURODYN 2017, 199: 3546–51. https://doi.org/10.1016/j.proeng.2017.09.512.

Harris, Angie, Xiang Y., Naeim, F., and Zareian, F. (2015). Identification And Validation of Natural Periods and Modal Damping Ratios for Steel and Reinforced Concrete Buildings in California. *SMIP15 Seminar Proceedings*.

Henry, Richard S., Dizhur, D., Elwood, K. J., Hare, J., and Brunsdon, D (2017). Damage to Concrete Buildings with Precast Floors during the 2016 Kaikoura Earthquake. *Bulletin of the New Zealand Society for Earthquake Engineering* 50, no. 2: 174–86. https://doi.org/10.5459/bnzsee.50.2.174-186.

Iverson, J. K., and Hawkins, N. M. (1994). Performance Of Precast/Prestressed Building Structures During Northridge Earthquake. *PCI Journal* 39, no. 2. https://trid.trb.org/view/390643.

Kam, W. Y., Pampanin, S., and Elwood, K. (2011). Seismic Performance of Reinforced Concrete Buildings in the 22 February Christchurch (Lyttleton) Earthquake. *University of Canterbury. Civil and Natural Resources Engineering*. https://ir.canterbury.ac.nz/handle/10092/9006.

Moaveni, Babak, He, X., Conte, J. P., Restrepo, J. I., and Panagiotou, M. (2011). System Identification Study of a 7-Story Full-Scale Building Slice Tested on the UCSD-NEES

Shake Table. *Journal of Structural Engineering* 137, no. 6: 705–17. https://doi.org/10.1061/(ASCE)ST.1943-541X.0000300.

Panagiotou, Marios, and Restrepo, J. I. (2009). Dual-Plastic Hinge Design Concept for Reducing Higher-Mode Effects on High-Rise Cantilever Wall Buildings. *Earthquake Engineering & Structural Dynamics* 38, no. 12: 1359–80. https://doi.org/10.1002/eqe.905.

Panagiotou, Marios, Restrepo, J. I., and Conte, J. P. (2011). Shake-Table Test of a Full-Scale 7-Story Building Slice. Phase I: Rectangular Wall. *Journal of Structural Engineering* 137, no. 6: 691–704. https://doi.org/10.1061/(ASCE)ST.1943-541X.0000332.

Priestley, M. J., and Alejandro D. Amaris (2012). *Dynamic Amplification of Seismic Moments and Shear Forces in Cantilever Walls*. IUSS Press.

Şafak, Erdal, and Çelebi, M (1990). Method to Estimate Center of Rigidity Using Vibration Recordings. *Journal of Structural Engineering* 116, no. 1: 85–97. https://doi.org/10.1061/(ASCE)0733-9445(1990)116:1(85).

Scarry, J M (2014). Floor Diaphragms – Seismic Bulwark or Achilles' Heel. *NZSEE Conference*, Auckland, New Zealand.

Sewell, R. T., Cornell, C. A., Toro, G. R., and McGuire, R. K. (1986). A Study of Factors Influencing Floor Response Spectra in Nonlinear Multi-Degree-of-Freedom Structures. *John A. Blume Earthquake Engineering Center Technical Report Series*. https://purl.stanford.edu/vf765pj9489.

The Pandas Development Team (2020). Pandas-dev/pandas: Pandas. *Zenodo*. https://doi.org/10.5281/zenodo.3509134.

Tilt-up-Wall Buildings. (1996). *Earthquake Spectra* 12, no. 1 (suppl): 99–123. https://doi.org/10.1193/1.1585922.

Tsampras, Georgios, Sause, R, Zhang, D., Fleischman, R. B, Restrepo, J. I., Mar, D., and Maffei, J. (2016). Development of Deformable Connection for Earthquake-Resistant Buildings to Reduce Floor Accelerations and Force Responses. *Earthquake Engineering & Structural Dynamics* 45, no. 9: 1473–94. https://doi.org/10.1002/eqe.2718.

Van Rossum, G., & Drake, F. L. (2009). Python 3 Reference Manual. Scotts Valley, CA: CreateSpace.

Wallace, John W., Massone, L. M., Bonelli, P., Dragovich, J., Lagos, R., Lüders, C., and Moehle, J. (2012). Damage and Implications for Seismic Design of RC Structural Wall Buildings. *Earthquake Spectra* 28, no. 1(supl): 281–99. https://doi.org/10.1193/1.4000047.

Wiebe, L., and Christopoulos, C. (2009). Mitigation of Higher Mode Effects in Base-Rocking Systems by Using Multiple Rocking Sections. *Journal of Earthquake Engineering* 13, no. sup1: 83–108. https://doi.org/10.1080/13632460902813315.

Xiang, Yijun, Harris, A., Naeim, F., and Zareian, F. (2016). Identification And Validation of Natural Periods and Modal Damping Ratios for Seismic Design and Building Code. *SMIP16 Seminar Proceedings*.